PCCP

ROYAL SOCIETY OF CHEMISTRY

PAPER

View Article Online
View Journal | View Issue

Cite this: *Phys. Chem. Chem. Phys.*, 2025, **27**, 18917

Structures and energetics of protonated bipyridine–cucurbituril complex isomers in the gas phase

Doui Kim[a] and Jongcheol Seo *[ab]

Received 14th July 2025,
Accepted 23rd August 2025

DOI: 10.1039/d5cp02677f

rsc.li/pccp

We investigated the gas-phase isomerism and stability of host–guest complexes formed between cucurbiturils (CB[6] and CB[7]) and three *n*,*n*′-bipyridine regioisomers (*n* = 2, 3, and 4), focusing on how molecular geometry and charge distribution influence complex formation. Ion mobility spectrometry-mass spectrometry and collision-induced dissociation experiments, supported by density functional theory (DFT) calculations, reveal distinct inclusion and exclusion complex isomers. Singly-protonated bipyridines tend to form exclusion complexes with CB[6], while doubly-protonated forms enable stable inclusion through enhanced charge–portal interactions. CB[7], with its larger and more flexible cavity, consistently supports inclusion for all bipyridine isomers, regardless of charge state. These findings emphasize the importance of charge localization, host flexibility, and phase-specific effects in supramolecular assembly, which may further offer valuable insights for designing bipyridine- or bipyridinium-based materials.

1. Introduction

In supramolecular chemistry, particularly during the formation of host–guest complexes, non-covalent interactions play a pivotal role in determining overall complex stability. However, for cavity-containing hosts such as cucurbiturils (CBs), pillararene, and cyclodextrins, it is not only the direct interactions between host and guest that matter, but also factors such as guest solvation in solution. In the case of CBs, which possess a confined cavity, a key driving force behind complex formation is the displacement of so-called ''high-energy water'', partially hydrogen-bonded water molecules within the cavity, upon guest inclusion.[1–3] In contrast, under solvent-free gas-phase conditions, host–guest complexes may adopt structures markedly different from those found in solution. This discrepancy can be especially pronounced in complexes involving CBs and cationic guests, where charge-dipole interactions between the positively charged guest and the portal region of the CB significantly influence complex stability.[4–7] In the absence of solvent-mediated charge screening, these electrostatic interactions become far more pronounced in the gas phase than in solution. As a result, a variety of host–guest complex isomers, which are distinct from those anticipated in solution, may be observed under gas-phase conditions.

Elucidating such gas-phase isomers and probing their energetics and stability are crucial for deepening our understanding of host–guest interactions. Recently, these gas-phase studies have been conducted effectively using ion mobility spectrometry-mass spectrometry (IMS-MS) in combination with electrospray ionization (ESI).[6,8–16] While mass spectrometry clearly identifies the stoichiometry of host–guest complexes, collision cross section (CCS) values obtained from IMS can reveal isomerism, such as whether the guest resides within the host cavity. For example, Dearden and co-workers used IMS-MS to distinguish the inclusion and exclusion complexes of CB[6]-phenylenediamine isomers.[17] Work by Nau and co-workers demonstrated that protonated azoalkanes form 1 : 1 inclusion complexes with CB[*n*] by comparing CCS values of the complex ions with those of empty CB[*n*] ions.[8] Kim and co-workers similarly employed IMS-MS to confirm the inclusion of alkylammonium ions in CB[*n*] cavities.[6] Recently, our group showed that IMS-MS effectively captures isomerism in various host–guest complexes, including the formation of alkali halide clusters, the protonation isomers of the imipramine-CB[7] complex, and the transition from bucket-wheel to tetrahedral assembly in cyclodextrin tetramers upon addition of alkali halide clusters.[14,16] Furthermore, we found that alkali halide cluster cations form inclusion complexes with CB[7] during the ESI process.[13]

Despite these pioneering gas-phase studies, relatively few investigations have explored how host–guest complexes differ when formed in the gas phase as opposed to in solution. In

[a] *Department of Chemistry, Pohang University of Science and Technology (POSTECH), Pohang, Gyeongsangbuk-do 37673, Republic of Korea. E-mail: jongcheol.seo@postech.ac.kr*
[b] *School of Interdisciplinary Bioscience and Bioengineering (I-BIO), Pohang University of Science and Technology (POSTECH), Pohang, Gyeonsangbuk-do 37673, Republic of Korea*

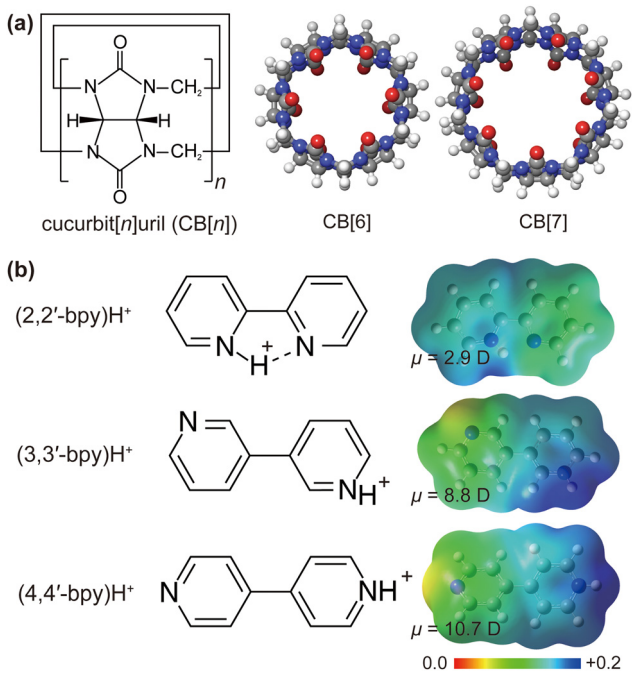

Fig. 1 (a) Structures of cucurbit[*n*]turils (*n* = 6 and 7), and (b) protonated *n*,*n*′-bipyridines (***n*bpy**·H^+, *n* = 2, 3, and 4) and their electrostatic potential map. The region mapped with blue surface represents the positively charged area. The dipole moments (μ, unit: Debye) of protonated bipyridines are given as well.

particular, more work is needed to determine which isomers can arise based on the location of the charge during gas-phase complex formation and how these structures correlate with those observed in solution. Additionally, further study is required to investigate how guests capable of adopting multiple structural isomers influence the formation of distinct host–guest complexes under solvent-free conditions. Detailed host–guest interactions influenced by guest molecular geometry, charge location, host cavity structure, and many more should be carefully examined in the gas phase to fully understand the host–guest interactions.

In this study, we focus on the isomerism of host–guest complexes formed between bipyridine and cucurbiturils (CBs) in the gas phase. Specifically, we examine how *n*,*n*′-bipyridines (***n*bpy**; *n* = 2, 3, or 4) form different complex isomers with CB[6] and CB[7] (Fig. 1). In CB-based systems, charge–portal interactions are key; the effectiveness of these interactions can strongly impact host–guest complex stability in the gas phase. Therefore, we employ bipyridine isomers as model guests to investigate the role of charge location in gas-phase host–guest complex formation. The three positional isomers of bipyridines exhibit marked differences in charge distribution and molecular dipole upon protonation (Fig. 1b). Although these isomers share a similar molecular shape, their varying charge distributions can lead to distinct modes of complexation in the gas phase. We also explore how complex formation differs between singly- and doubly-protonated bipyridines, thereby illuminating how charge distribution affects the stability of these host–guest assemblies in the gas phase. Furthermore, using collision cross-section (CCS) values obtained from IMS-MS together with density functional theory (DFT) calculations, we predicted possible isomeric structures and then evaluated their gas-phase stability *via* collision-induced dissociation (CID). By integrating these experimental and theoretical approaches, we aim to elucidate the driving forces governing the formation and stability of bipyridine–CB complexes in the gas phase, with a particular focus on bipyridine isomerism and the cavity size of the CB hosts.

2. Experimental section

2.1. Sample preparation

All chemicals except cucurbiturils were purchased from Sigma-Aldrich (St. Louis, MI, USA) and used without further purification. Cucurbiturils (CB[6] and CB[7]) were generously synthesized and provided by Prof. Kimoon Kim's group. The sample solutions for the ESI-IMS-MS were prepared by dissolving CB (CB[6] or CB[7]) and *n*,*n*′-bipyridine in pure water or water/acetonitrile (1/1, v/v) to a final concentration of 50 μM for both CB and *n*,*n*′-bipyridine. A small amount of aqueous HCl or KCl solution was added to increase H^+ or K^+ concentration to enhance the formation of doubly-charged complex ions. The sample solution for the nuclear magnetic resonance (NMR) experiment was prepared similarly, but with elevated concentrations (1 mM for both CB and *n*,*n*′-bipyridine) in D_2O. A small amount of DCl was added to acidify the solution.

2.2. Electrospray ionization-ion mobility spectrometry-mass spectrometry (ESI-IMS-MS)

IMS-MS experiments were done by using ion mobility-quadrupole time-of-flight instrument (6560 IM-Q-TOF, Agilent Technologies Inc., Santa Clara, CA, USA) equipped with a home-built nanoelectrospray ionization (*n*ESI) source. An aliquot (5 μL) of the prepared sample solution was loaded into the custom Au-coated borosilicate emitter prepared by micropipette puller (P-1000, Sutter Instrument Inc., Novato, CA, USA), and sprayed with a voltage offset of 0.8–1.5 kV between the emitter tip and inlet capillary. Heated N_2 drying gas (120 °C, flow rate of 2.5 L min^{-1}) was introduced to enhance the ESI process. Ions generated during the experiment were confined in the entrance ion funnel for 1 ms before being pulsed into an 80-cm-long drift tube filled with nitrogen buffer gas (~3.95 torr). Within the drift tube, the ions travelled under a constant electric field (10–15 V cm^{-1}), enabling their separation based on collision cross section and charge state. The separated ions were subsequently focused in the exit ion funnel and transported to a high-vacuum region, where time-of-flight (TOF) mass spectra were acquired for the ions separated by ion mobility at intervals of 150 μs. To construct the arrival time distribution (ATD) of a specific ion, the ion signals for a selected mass-to-charge ratio (*m*/*z*) were extracted from the series of TOF spectra and plotted against the time delay between ion introduction into the drift tube and TOF detection. The experimental collision cross section (CCS) for a specific *m*/*z* ion was determined from its measured arrival time using the

stepped-field method. In this approach, the arrival times (t_d) of the analyte ion were recorded at different drift tube voltage differences (drift voltage, V_d). A plot of t_d *versus* $1/V_d$ was then generated, and the ion mobility (K) was calculated through linear regression. The CCS value was subsequently derived from the mobility using the Mason-Schamp equation. Details are given in the SI.

2.3. Collision-induced dissociation

A specific CB-bipyridine complex ion was isolated by its m/z value at the quadrupole mass filter after the ion mobility separation. The m/z-selected ions were accelerated by applying an acceleration voltage (V_{CE}) just before the collision cell filled with N_2 collision gas ($\sim 1.5 \times 10^{-4}$ torr). Multiple collisions of m/z-selected ions with N_2 collision gas molecules convert the acquired kinetic energy into internal energy, subsequently inducing dissociation of collisionally activated ions. The product ion mass spectra were obtained by varying the acceleration voltage. The fractions of precursor and product ions were plotted as a function of relative collision energy (RCE), where RCE = $z \cdot V_{CE}$ (z = charge state of precursor ion).

2.4. Theoretical calculations

All density functional theory (DFT) calculations were done by using Gaussian 16 program suite.[18] The geometries of various singly- or doubly-protonated 1 : 1 CB[x]-(n,n'-bipyridine) complex ions (x = 6 or 7, n = 2, 3, or 4) were optimized using PBE0 level[19] of DFT with cc-pVDZ basis set. The Grimme D3 dispersion correction[20] was applied to attribute the long-range interactions, which are common for non-covalent host–guest interactions. Basis set superposition errors were corrected by the counterpoise method[21] to accurately evaluate the binding energies between CB and bipyridines.

Harmonic vibrational frequencies and zero-point vibrational energies were calculated with the same theoretical level and scaled by 0.984,[22] and further used for evaluating thermodynamic quantities such as enthalpies and Gibbs free energies. Partial charges of atoms in the optimized geometry were calculated by fitting the electrostatic potential using Merz–Singh–Kollman scheme,[23] which were further used to predict theoretical CCS. The theoretical CCS values of the optimized isomer geometries under the N_2 drift gas were calculated by trajectory methods with considering both ion-dipole and ion-quadrupole interactions[24,25] implemented in iMoS program (version 1.13).[26] The optimized Lennard-Jones potential parameters were used for trajectory method calculations. (Table S1)

3. Results

3.1. Singly- and doubly-protonated cucurbituril-bipyridine complex isomers observed by IMS-MS

As shown in Fig. 2a, CB[6] readily forms both singly- and doubly-protonated 1 : 1 complex ions with n,n'-bipyridines (***n*bpy**; n = 2, 3, or 4), namely CB[6]·***n*bpy**·H^+ (m/z 1153) and CB[6]·***n*bpy**·H_2^{2+} (m/z 577). However, the formation of CB[6]·**2bpy**·H_2^{2+} is significantly less abundant compared to the other isomers. The arrival time distributions (ATDs) of CB[6]·***n*bpy**·H^+ ions show clear isomeric differences depending on the

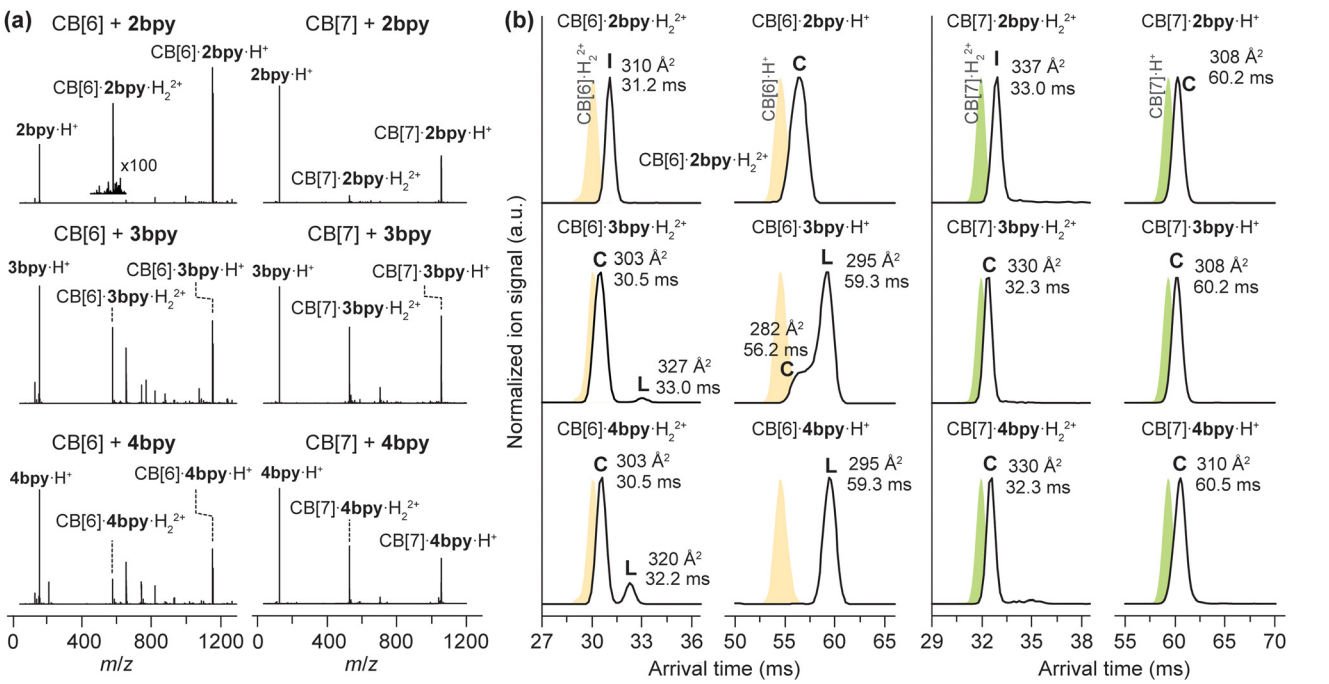

Fig. 2 (a) ESI-MS spectra of the solution containing CB[6]-(n,n'-bipyridine) (left) and CB[7]-(n,n'-bipyridine) (right). (b) The arrival time distributions (ATDs) of singly- and doubly-protonated CB[6]-bipyridine (left) and CB[7]-bipyridine complexes (right) The ATDs of protonated CB[6] (CB[6]·H_2^{2+} and CB[6]·H^+) and protonated CB[7] (CB[7]·H_2^{2+} and CB[7]·H^+) are shown together as yellow and green shades, respectively. Depending on the arrival time, the observed ATD peaks are grouped into isomers **C** (compact), **L** (large), or **I** (intermediate). Determined collision cross section values are given as well.

bipyridine isomer. CB[6]·**2bpy**·H^+ displays a single peak at 56.2 ms, while CB[6]·**4bpy**·H^+ appears at 59.3 ms. In contrast, CB[6]·**3bpy**·H^+ shows two peaks: a minor one at 56.2 ms and a major one at 59.3 ms, suggesting the coexistence of two isomers resembling those of CB[6]·**2bpy**·H^+ and CB[6]·**4bpy**·H^+. Considering the ATD of guest-free CB[6]·H^+ at 53.5 ms (corresponding to a CCS of ~272 Å^2), the isomers at 56.2 ms (group **C**, CCS ~282 Å^2) may be tentatively assigned to inclusion complexes, where the guest resides inside the cavity. Conversely, the longer ATD of 59.3 ms (group **L**, CCS ~295 Å^2) can be clearly assigned to exclusion complexes, in which the guest lies outside the host cavity. Therefore, CB[6]·**2bpy**·H^+ and part of CB[6]·**3bpy**·H^+ are presumably inclusion complexes, while CB[6]·**4bpy**·H^+ and the major CB[6]·**3bpy**·H^+ isomer form exclusion complexes.

In the doubly-protonated series, CB[6]·***n*bpy**·H_2^{2+} ions display mostly compact structures. CB[6]·**3bpy**·H_2^{2+} and CB[6]·**4bpy**·H_2^{2+} each show two isomers: a major species at 30.5 ms (group **C**, CCS ~303 Å^2) and a minor one at 33.0 or 32.2 ms (group **L**, CCS ~327 Å^2 or 320 Å^2, respectively). CB[6]·**2bpy**·H_2^{2+}, despite its low abundance, displays a single ATD peak at 31.2 ms (CCS ~310 Å^2), intermediate (**I**) between group **C** and **L**, suggesting partial guest encapsulation rather than full inclusion or exclusion. When compared to the doubly protonated CB[6]·H_2^{2+} ion at 29.8 ms (298 Å^2), group **C** isomers are assigned as inclusion complexes. These findings indicate that double protonation facilitates bipyridine encapsulation even within the spatially restricted CB[6] cavity.

Interestingly, the inclusion complexes of singly protonated CB[6]·***n*bpy**·H^+ species increase the CCS by ~4% relative to free CB[6]·H^+, whereas those of doubly protonated CB[6]·***n*bpy**·H_2^{2+} increase it by only ~1.6%. This suggests deeper guest embedding in the doubly protonated complexes, while singly protonated bipyridines remain partially exposed. These observations highlight the critical role of charge in stabilizing gas-phase inclusion complexes. While single protonation is insufficient to retain **3bpy** and **4bpy** inside the CB[6] cavity, double protonation enables favorable charge–portal interactions at both ends of the guest, overcoming steric constraints and allowing full encapsulation.

In contrast, CB[7] forms stable inclusion complexes with all three bipyridines, regardless of protonation state. As shown in Fig. 3a, both CB[7]·***n*bpy**·H^+ (*m*/*z* 1319) and CB[7]·***n*bpy**·H_2^{2+} (*m*/*z* 660) ions are abundantly observed. For the singly-protonated species, a single ATD peak (group **C**) is observed

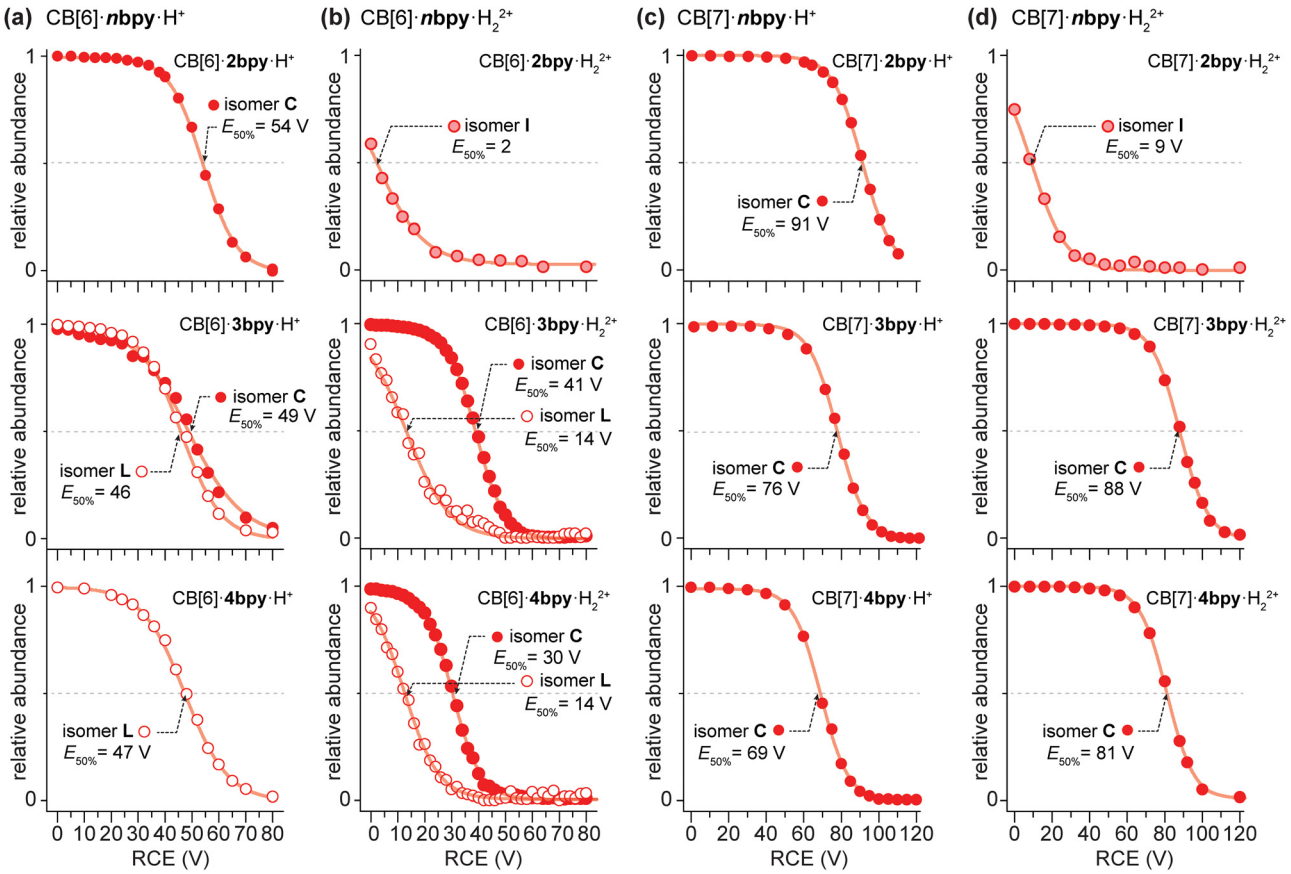

Fig. 3 The energy-dependent survival yield of precursor ions, the singly- and doubly-protonated CB[*x*]-bipyridine complexes (*x* = 6 or 7): (a) CB[6]·***n*bpy**·H^+, (b) CB[6]·***n*bpy**·H_2^{2+}, (c) CB[7]·***n*bpy**·H^+, and (d) CB[7]·***n*bpy**·H_2^{2+} (*n* = 2, 3, and 4 for top, middle, and bottom, respectively). Red lines denote the sigmoidal fits of the precursor (CB[*x*]-bipyridine complex ions) depletion. RCE denotes the relative collision energy (RCE = $z \cdot V_{CE}$), where *z* is the charge state of complex ion and V_{CE} is acceleration voltage before entering the collision cell. For each isomer, the RCE for 50% precursor dissociation ($E_{50\%}$) value is shown together.

for all regioisomers, with CCS values nearly identical to CB[7]·H^+ (~305 Å^2), indicating inclusion complexes. In the doubly protonated series, CB[7]·**3bpy**·H_2^{2+} and CB[7]·**4bpy**·H_2^{2+} exhibit dominant isomers with CCS values similar to CB[7]·H_2^{2+}, further supporting encapsulation. However, CB[7]·**2bpy**·H_2^{2+} displays a slightly larger CCS (~337 Å^2), suggesting the guest is only partially encapsulated, consistent with the behavior of CB[6]·**2bpy**·H_2^{2+}.

No exclusion-type (group **L**) isomers are observed for CB[7]-based complexes, emphasizing the impact of host cavity size on complexation behavior. The larger cavity of CB[7] accommodates bipyridines more efficiently, promoting inclusion even for singly protonated guests, unlike the more size-constrained CB[6].

3.2. Dissociation energetics of cucurbituril-bipyridine complex ions in the gas phase

To gain further insight into the gas-phase stability of the CB-bipyridine complexes, we conducted energy-resolved collision-induced dissociation (CID) experiments (Fig. 3). The resulting survival yields were used to extract the center-of-sigmoid voltage ($E_{50\%}$), reflecting the energy required to fragment 50% of the precursor ions. Representative product ion spectra are provided in Fig. S1–S4.

For singly protonated CB[6]·***n*bpy**·H^+ complexes (Fig. 3a), dissociation proceeds primarily *via* proton transfer from bipyridine to the CB[6] portal, yielding CB[6]·H^+ and neutral bipyridine (Fig. S1). Since the gas-phase proton affinities of CBs can be enhanced by sharing a proton by two or three portal carbonyls, the proton transfer from bipyridine to the CB portal can be favorable. Notably, the **L** isomers of CB[6]·**3bpy**·H^+ and CB[6]·**4bpy**·H^+, assigned as exclusion complexes, exhibit nearly identical dissociation profiles ($E_{50\%}$ = 46–47 V). The **C** isomer of CB[6]·**3bpy**·H^+, attributed to an inclusion structure, requires slightly higher energy ($E_{50\%}$ = 49 V), suggesting marginally enhanced stability. The CB[6]·**2bpy**·H^+ complex (isomer **C**) dissociates at a noticeably higher energy ($E_{50\%}$ = 54 V), likely due to a different mechanism: in this case, **2bpy**·H^+ is ejected from the cavity without prior proton transfer (Fig. S1), reflecting the intrinsic stability of the proton on **2bpy**, stabilized by both nitrogen atoms. These results suggest that, for singly-protonated complexes, the dissociation energetics are largely governed by the ease of proton transfer rather than inclusion geometry.

In contrast, doubly protonated CB[6]·***n*bpy**·H_2^{2+} complexes exhibit pronounced isomer-specific dissociation behavior (Fig. 3b). The inclusion isomers (isomer **C**) of CB[6]·**3bpy**·H_2^{2+} and CB[6]·**4bpy**·H_2^{2+} require significantly more energy to dissociate ($E_{50\%}$ = 41 V and 30 V, respectively) compared to their exclusion isomers (isomer **L**) ($E_{50\%}$ = 14 V). The dissociation pathway involves charge separation into CB[6]·H^+ and ***n*bpy**·H^+ (Fig. S2). The higher stability of the inclusion isomers indicates that dual charge–portal interactions stabilize the encapsulated bipyridines. Interestingly, CB[6]·**3bpy**·H_2^{2+} shows greater stability than CB[6]·**4bpy**·H_2^{2+}, highlighting the influence of proton location on complex energetics.

The CB[6]·**2bpy**·H_2^{2+} complex (isomer **I**) displays the lowest stability among the doubly charged species ($E_{50\%}$ = 2 V). Given the unfavorable double protonation on **2bpy** due to strong Coulombic repulsion, it is likely that one proton resides on the guest and the other on CB[6], weakening the overall binding. The same may apply to the **L** isomers of CB[6]·**3bpy**·H_2^{2+} and CB[6]·**4bpy**·H_2^{2+}, in which minimal host–guest interactions result in lower dissociation energies.

These findings suggest that the inclusion isomers of CB[6]·***n*bpy**·H_2^{2+} consist of a doubly protonated bipyridine stabilized within a neutral CB[6] host, whereas the exclusion or partially bound forms distribute charge between host and guest. The additional proton in the doubly-charged complexes is thus critical for stabilizing inclusion complexes, particularly for **3bpy** and **4bpy**.

For CB[7]-bipyridine complexes (Fig. 3c and d), dissociation pathways are similar to those CB[6]-bipyridine complex ions (Fig. S3 and S4). However, dissociations of CB[7]-bipyridine complex ions generally require higher collision energy than their CB[6] counterparts, consistent with stronger host–guest interactions afforded by the larger cavity. It should be noted that the direct $E_{50\%}$ comparison between CB[6]-bipyridine and CB[7]-bipyridine complex ions is not feasible due to their different vibrational degrees of freedom. Nevertheless, the $E_{50\%}$ values of CB[7]-bipyridine complex ions are significantly higher (>50%) than those of CB[6]-bipyridine complex ions, even considering the differences in the vibrational degrees of freedom. Singly protonated CB[7]·***n*bpy**·H^+ isomers dissociate at $E_{50\%}$ values of 91 V (**2bpy**), 76 V (**3bpy**), and 69 V (**4bpy**), all assigned as inclusion isomers (isomer **C**). This trend supports the notion that CB[7] can accommodate bipyridines more effectively than CB[6]. Doubly-protonated CB[7]·***n*bpy**·H_2^{2+} complexes exhibit similar behavior, with inclusion isomers (isomer **C**) dissociating at $E_{50\%}$ = 88 V (**3bpy**) and 81 V (**4bpy**), again indicating strong stabilization. The CB[7]·**2bpy**·H_2^{2+} complex (isomer **I**) shows largely reduced stability ($E_{50\%}$ = 9 V), consistent with CB[6]·**2bpy**·H_2^{2+} case.

In summary, the dissociation energetics highlight the cooperative effects of charge and cavity size on gas-phase complex stability. While CB[6] relies on charge-enhanced portal interactions to stabilize inclusion complexes, CB[7] forms robust inclusion complexes more universally. Moreover, the position of the proton(s) on bipyridine critically modulates host–guest interaction strength, particularly in the spatially constrained CB[6] cavity.

3.3. Theoretically predicted gas-phase structures and stabilities of cucurbituril-bipyridine complex isomers

To complement the experimental IMS-MS and CID results, we performed density functional theory (DFT) calculations to predict the low-energy structures and dissociation pathways of the singly- and doubly-protonated CB bipyridine complex ions (Fig. 4). For each singly- and doubly-protonated complex, we evaluated both inclusion and exclusion configurations and compared their relative Gibbs free energies in the gas phase and theoretical CCS values.

The calculated structures align well with the experimentally observed isomer types: the inclusion structures correspond to the experimentally identified **C** isomers, while the exclusion structures match the **L** isomers. As shown in Fig. 4a, for CB[6]·**2bpy**·H^+, the inclusion complex is significantly more stable than the exclusion form ($\Delta G_{298\,K}$ = −200.2 *vs.* −104.6 kJ mol^{-1}), consistent with the dominant population of isomer **C** in the ATDs. In contrast, for CB[6]·**3bpy**·H^+ and CB[6]·**4bpy**·H^+, the exclusion complexes are predicted to be energetically favored, in agreement with the strong presence of isomer **L** in the experiments. Notably, for CB[6]·**3bpy**·H^+, the inclusion complex is only slightly less stable (∼8.8 kJ mol^{-1} higher in $\Delta G_{298\,K}$), and its minor presence (isomer **C**) is consistent with this small energy difference. In the case of doubly-protonated CB[6]-bipyridine complexes (Fig. 4b), inclusion complexes are predicted to be significantly more stable than exclusion complexes for all three bipyridine isomers. This agrees with the dominant observation of inclusion-type **C** isomers in the ATDs and their enhanced stability in CID experiments. These findings highlight that additional protonation reinforces charge–portal interactions, favoring guest encapsulation even in the sterically constrained CB[6] cavity. In case of the CB[6]·**2bpy**·H_2^{2+}, meanwhile, exhibit half-inclusion complex while CB[6]·**3bpy**·H_2^{2+} and CB[6]·**4bpy**·H_2^{2+} are forming full-inclusion complexes

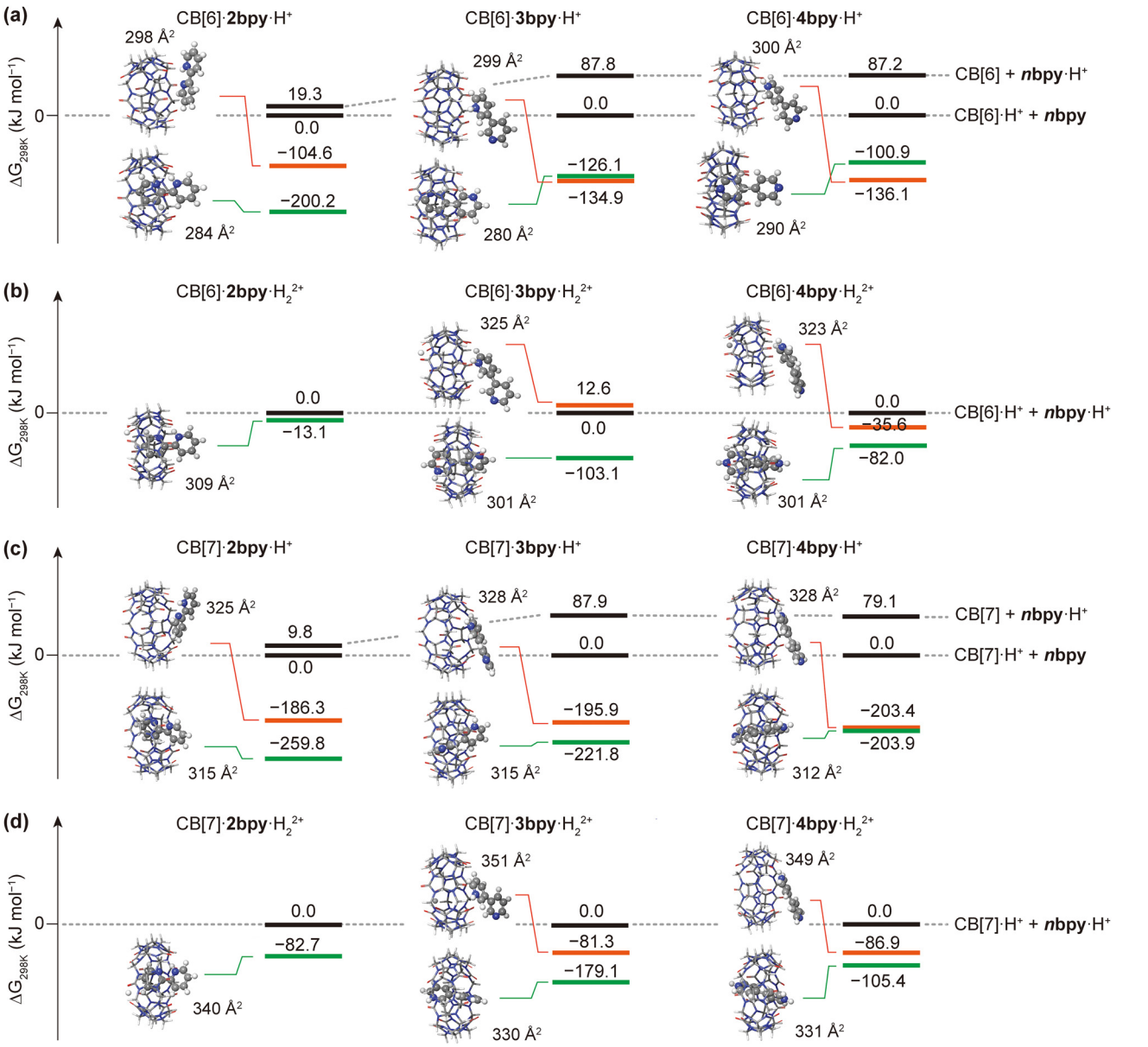

Fig. 4 The low-energy structures of CB[*x*]-bipyridine complex ions (*x* = 6 or 7) predicted by density functional theory in the gas phase: (a) CB[6]·***n*bpy**·H^+, (b) CB[6]·***n*bpy**·H_2^{2+}, (c) CB[7]·***n*bpy**·H^+, and (d) CB[7]·***n*bpy**·H_2^{2+} (*n* = 2, 3, and 4 for left, center, and right, respectively). Lowest-energy structures for both Inclusion and exclusion complexes are shown with their relative binding Gibbs free energies and predicted collision cross section values. The detailed molecular geometries are given in SI (Fig. S5–S8).

(Fig. 4c), which is in line with our experimental observation of intermediate **I** isomer.

For CB[7]·***n*bpy**·H^+ and CB[7]·***n*bpy**·H_2^{2+} complexes (Fig. 4c and d), inclusion complexes are consistently more stable across all bipyridine isomers, with $\Delta G_{298\,K}$ differences exceeding 70 kJ mol^{-1} in most cases. The larger CB[7] cavity accommodates the bipyridine guest more readily, explaining why only inclusion isomers were observed experimentally, regardless of regioisomer or charge state. Once again, the most stable structure of CB[6]·**2bpy**·H_2^{2+} has half-included **2bpy**, which is well assigned to the intermediate **I** isomer. This emphasizes the impact of charge location of the protonated guest on the complex structure in the gas phase where the electrostatic interactions become dominant. Altogether, the DFT-predicted energetics correlate well with the experimental IMS-MS and CID results, confirming that gas-phase host–guest isomer distributions largely follow thermodynamic stability in the gas phase. Charge location, bipyridine geometry, and host cavity size collectively dictate whether inclusion or exclusion structures dominate in the gas phase.

Notably, as shown in Fig. 5, the inclusion complex of CB[6] with bipyridine (CB[6]·**4bpy**·H_2^{2+}, representatively) exhibits an optimized gas-phase structure in which the guest is well-aligned along the principal axis of the host. However, to accommodate the rigid bipyridine molecule, CB[6] undergoes noticeable flattening, resulting in a distorted, compressed conformation. Since DFT calculation estimates that the deformation of CB[6] is ~23 kJ mol^{-1} less stable than the undeformed CB[6], the inclusion of bipyridine in CB[6] itself is intrinsically unfavorable in the gas phase unless charge–portal interactions compensate the energetic disadvantage. In contrast, in the CB[7]-bipyridine inclusion complex (CB[7]·**4bpy**·H_2^{2+}, representatively in Fig. 5), the host retains a more symmetric and less distorted shape, while the bipyridine guest adopts a tilted (~15°) orientation within the cavity. DFT calculation estimates that this guest tilting provides an energetic gain of ~58 kJ mol^{-1}. These distinct structural features, showing host distortion in CB[6] complexes and guest tilting in CB[7] complexes, appear to be critical determinants of the complex stability in the gas phase.

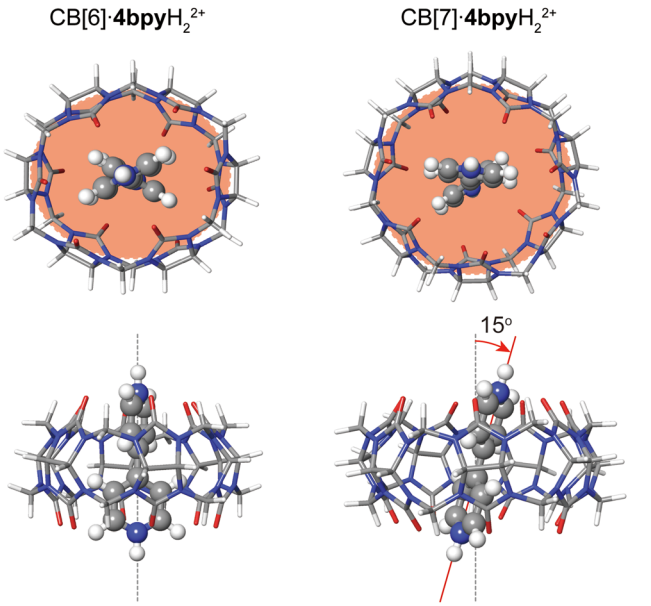

Fig. 5 Detailed structure displays (top and side views) of the optimized CB[6]·**4bpy**·H_2^{2+} and CB[7]·**4bpy**·H_2^{2+} inclusion complex ions.

4. Discussion

4.1. Impact of the molecular geometry on the host–guest complex stability in the gas phase

Compared to CB[6], CB[7] possesses a larger cavity, which allows more favorable accommodation of guests without large cavity distortion in the gas phase by optimizing cation–portal interactions. Although bipyridine molecules are slightly larger than the portal-to-portal distance of cucurbiturils, doubly-protonated guests can still be partially inserted into the cavity, because the guest bipyridine can be tilted inside the cavity. In CB[6], however, the restricted internal space imposes large steric hindrance that forces larger structural distortion to accommodate a bipyridine guest. Moreover, limited cavity size inhibits the tilting of bipyridine, making it difficult to fully optimize cation–portal interactions. This tilting of the bipyridine guest in CB[7] cavity facilitates simultaneous interaction of both terminal nitrogen atoms with the carbonyl-rich portals, thereby stabilizing the inclusion complex more effectively than in CB[6]. The observed differences in gas-phase complexation behavior between CB[6] and CB[7] thus arise from their differing structural flexibility and cavity sizes. This interpretation is consistent with prior studies by Kim and co-workers, who examined the gas-phase inclusion of α,ω-alkylammonium ions in CB[6] and CB[7].[6] In those systems, the guests were less bulky and more conformationally flexible than bipyridines, enabling favorable inclusion complexes with both CB[6] and CB[7] hosts. In contrast, bipyridines exhibit greater intrinsic rigidity than alkylammoniums, making the cucurbituril's cavity size and flexibility crucial factors in stabilizing the inclusion complex.

However, the enhanced charge–portal interaction in the gas phase serves as a strong driving force that can overcome unfavorable structural factors. For instance, in the case of CB[6]·**4bpy**·H^+, the inclusion complex is less stable than the exclusion complex. DFT-optimized structures indicate that only the protonated pyridyl ring is inserted into the CB[6] cavity to minimize steric hindrance. In contrast, the doubly protonated CB[6]·**4bpy**·H_2^{2+} complex forms a more stable inclusion complex, which is also observed experimentally. Despite the structural limitation that prevents **4bpy**·H_2^{2+} from effectively engaging in close-range interactions with the carbonyl-lined portals of CB[6], the complex still adopts an inclusion geometry, indicating that the additional positive charge provides sufficient stabilization to offset steric repulsion. This observation highlights the role of double protonation in reinforcing charge–portal interactions at both ends of the CB cavity, effectively promoting inclusion complex formation in the gas

phase. A similar principle explains why CB[6]·**3bpy**·H_2^{2+} forms a more stable complex than CB[6]·**4bpy**·H_2^{2+}. Structurally, the distance between the protonated nitrogen atoms is shorter in **3bpy** than in **4bpy**, allowing better alignment with the portals. Additionally, the tilted geometry of **3bpy** allows more favorable interactions with the carbonyl oxygens compared to the linear axis-aligned structure of **4bpy**. More specifically, the singly- and doubly-protonated **3bpy** in the CB cavity have charges more closely and strongly solvated by two or three portal carbonyl oxygens. In case of the protonated **4bpy**, conversely, the charge is solvated weakly by entire portal carbonyl oxygens unless **4bpy** is tilted inside the CB cavity.

Together, these findings indicate that the gas-phase stability of CB-bipyridine complexes in the gas phase arises from a delicate balance between structural distortion, steric constraints, and charge localization. Double protonation, in particular, enhances portal binding interactions and can compensate for structural mismatches between host and guest, thereby enabling inclusion complexation even in sterically constrained environments.

4.2. Relevance to the solution phase isomers

To compare the gas-phase findings with solution-phase behavior, we performed ^{1}H NMR experiments under aqueous conditions (Fig. S9–S11). These results show that none of the bipyridines form significant inclusion complexes with CB[6]. For CB[7], only **4bpy** yields a clearly defined inclusion complex, while **3bpy** shows negligible interaction, and **2bpy** exhibits weak interactions towards inclusion. In contrast, gas-phase measurements reveal that doubly-protonated bipyridines form inclusion complexes with both CB[6] and CB[7], with CB-**3bpy** complexes often more stable than CB-**4bpy** complexes. This trend is opposite to what is observed in solution, where CB[7]-**4bpy** is supposed to be the most stable. In addition, the observations of doubly-protonated complexes are not relevant to the solution characteristics, either. Even accounting for p*K*a shifts upon complexation,[27] the formation of doubly-protonated bipyridine inclusion complexes in aqueous media remains unlikely due to electrostatic repulsion and solvation effects.

We attribute this discrepancy to two key factors. First, in solution, the portals of cucurbiturils can also be solvated, which weakens the impact of cation–portal interactions on the complex formation relative to the gas phase. Second, gas-phase conditions allow both host and guest to undergo slight structural distortions that enhance binding as mentioned previously: the CB host can contract or elongate, and the bipyridine can tilt to optimize electrostatic interactions. Such distortions are energetically unfavorable in solution, where the solvation shell imposes constraints on molecular flexibility.

Drawing on previous work showing that alkali halide clusters form inside CB[7] during electrospray droplet desolvation, we propose that the CB-bipyridine inclusion complex ions observed here arise as solvent is removed and charge–portal interactions strengthen, driving the bipyridine into the CB[6] cavity. For CB[7], only the **4bpy** inclusion complex seen in solution remains stable; other inclusion complexes are generated during the ESI process.

These findings underscore an important caution for host–guest studies. Although solution-phase complexes are often retained in the gas phase, guests with high charge density, such as doubly-protonated bipyridines, may form different inclusion complexes during electrospray when interacting with hosts like CB[6] or CB[7] that emphasize charge–portal binding.

4.3. Implications on the design of bipyridine-based supramolecular assemblies

The present study highlights how the molecular geometry and charge distribution of bipyridine isomers critically influence their ability to form stable inclusion complexes with cucurbiturils in the gas phase. Although the three bipyridine regioisomers share a similar backbone, their protonation patterns lead to markedly different charge localizations and dipole moments, which in turn determine whether they adopt inclusion or exclusion geometries within CB[6] or CB[7]. These findings suggest that even subtle changes in guest structure can result in significant variation in host–guest interaction modes. This insight indicates that, in supramolecular design, charge localization can serve as an effective handle for modulating host binding specificity, particularly in systems where electrostatic interactions play a dominant role. For example, these results are directly relevant to the design of functional supramolecular systems based on bipyridinium derivatives such as methyl viologen (MV^{2+}). MV is widely used in redox-active materials, pseudorotaxanes, and electrochromic polymers, where its strong affinity for cucurbiturils and well-defined dicationic structure play essential roles. The observation that inclusion complex stability depends sensitively on both charge state and host deformation suggests that the redox switching behavior of MV-based systems could be finely modulated by host selection and cavity engineering.

Taken together, our findings bridge fundamental gas-phase host–guest chemistry with the rational design of bipyridine-based functional materials. They emphasize the need to consider not only guest structure and charge state, but also host flexibility, environmental context, and the possible divergence between solution and gas-phase assembly pathways. Such knowledge will support the development of more robust and tunable supramolecular systems for applications in molecular electronics, sensing, ion recognition, and responsive materials.

5. Conclusions

In this study, we investigated the isomerism and stability of cucurbituril–bipyridine complexes in the gas phase using IMS-MS, energy-dependent CID, and DFT calculations. By systematically comparing three bipyridine regioisomers (**2bpy**, **3bpy**, and **4bpy**) and two cucurbiturils (CB[6] and CB[7]), we demonstrated how charge state, guest geometry, and host cavity size govern the formation and stability of inclusion *versus* exclusion complexes. Our results reveal that singly-protonated

bipyridines tend to form exclusion complexes with CB[6], while doubly-protonated species are more likely to be fully encapsulated, highlighting the critical role of electrostatic charge–portal interactions in the gas phase once again. CB[7], with its larger and more flexible cavity, consistently favors inclusion complexes regardless of the bipyridine isomer or charge state. The DFT-predicted structures and binding energetics are in excellent agreement with IMS and CID measurements, confirming that the observed gas-phase isomers correspond to thermodynamically favorable structures. However, the observed gas-phase structures are supposed not to reflect the host–guest interactions in solution. Comparison with solution-phase NMR experiments reveals notable discrepancies: while CB[7]-**4bpy** forms a stable inclusion complex in solution, most other CB-bipyridine complexes are expected to arise during the electrospray process. This highlights the unique influence of desolvation and structural relaxation on host–guest complexation in the gas phase, especially for rigid, multiply charged guests.

Overall, our findings underscore the importance of considering both molecular geometry and charge distribution when interpreting gas-phase host–guest interactions, particularly in systems involving rigid guests and highly electrostatically biased hosts like cucurbiturils. This work contributes to a deeper understanding of the structural dynamics governing host–guest chemistry across different phases and provides a framework for rationalizing ESI-generated complex ions beyond their solution-state behavior.

Author contributions

Doui Kim – data curation, formal analysis, and writing original draft; Jongcheol Seo – conceptualization, supervision, funding acquisition, project administration, and reviewing/editing manuscript.

Conflicts of interest

There are no conflicts to declare.

Data availability

The data supporting this article have been included as part of the SI. Supplementary information: (i) Detailed procedure for the experimental collision cross section (CCS) determination, (ii) optimized parameters for the theoretical CCS predictions, (iii) supplementary data providing product ion mass spectra of complex ions and ^{1}H NMR results, and (iv) detailed structures of theoretically optimized complex ions. See DOI: **https://doi.org/10.1039/d5cp02677f**

Acknowledgements

The authors are grateful for the financial support provided by the National Research Foundation of Korea (NRF), funded by the Ministry of Science and ICT (MSIT) (Grant No. RS-2019-NR041124 and RS-2020-NR049542). This work is also supported by the Basic Science Research Institute (BSRI), POSTECH under the NRF grant No. RS-2021-NR060139. D. Kim acknowledges the support from BK21 FOUR (Brain Korea 21 Fostering Outstanding Universities for Research), funded by the Ministry of Education (MOE) of Korea. We also thank to the Prof. Kyeng Min Park (Daegu Catholic University), Prof. Ilha Hwang (POSTECH), and Prof. Kimoon Kim (POSTECH) for providing the cucurbituril samples and for their fruitful discussion.

Notes and references

1 F. Biedermann, V. D. Uzunova, O. A. Scherman, W. M. Nau and A. De Simone, Release of High-Energy Water as an Essential Driving Force for the High-Affinity Binding of Cucurbit[n]urils, *J. Am. Chem. Soc.*, 2012, **134**, 15318–15323, DOI: **10.1021/ja303309e**.

2 F. Biedermann, M. Vendruscolo, O. A. Scherman, A. De Simone and W. M. Nau, Cucurbit[8]uril and Blue-Box: High-Energy Water Release Overwhelms Electrostatic Interactions, *J. Am. Chem. Soc.*, 2013, **135**, 14879–14888, DOI: **10.1021/ja407951x**.

3 K. I. Assaf and W. M. Nau, Cucurbiturils: from synthesis to high-affinity binding and catalysis, *Chem. Soc. Rev.*, 2015, **44**, 394–418, DOI: **10.1039/C4CS00273C**.

4 I. Osaka, M. Kondou, N. Selvapalam, S. Samal, K. Kim, M. V. Rekharsky, Y. Inoue and R. Arakawa, Characterization of host–guest complexes of cucurbit[n]uril (n = 6, 7) by electrospray ionization mass spectrometry, *J. Mass Spectrom.*, 2006, **41**, 202–207, DOI: **10.1002/jms.978**.

5 U. Rauwald, F. Biedermann, S. Deroo, C. V. Robinson and O. A. Scherman, Correlating Solution Binding and ESI-MS Stabilities by Incorporating Solvation Effects in a Confined Cucurbit[8]uril System, *J. Phys. Chem. B*, 2010, **114**, 8606–8615, DOI: **10.1021/jp102933h**.

6 S. J. C. Lee, J. W. Lee, H. H. Lee, J. Seo, D. H. Noh, Y. H. Ko, K. Kim and H. I. Kim, Host–Guest Chemistry from Solution to the Gas Phase: An Essential Role of Direct Interaction with Water for High-Affinity Binding of Cucurbit[n]urils, *J. Phys. Chem. B*, 2013, **117**, 8855–8864, DOI: **10.1021/jp4053874**.

7 S. J. Barrow, S. Kasera, M. J. Rowland, J. del Barrio and O. A. Scherman, Cucurbituril-Based Molecular Recognition, *Chem. Rev.*, 2015, **115**, 12320–12406, DOI: **10.1021/acs.chemrev.5b00341**.

8 T.-C. Lee, E. Kalenius, A. I. Lazar, K. I. Assaf, N. Kuhnert, C. H. Grün, J. Jänis, O. A. Scherman and W. M. Nau, Chemistry inside molecular containers in the gas phase, *Nat. Chem.*, 2013, **5**, 376–382, DOI: **10.1038/nchem.1618**.

9 F. Lanucara, S. W. Holman, C. J. Gray and C. E. Eyers, The power of ion mobility-mass spectrometry for structural characterization and the study of conformational dynamics, *Nat. Chem.*, 2014, **6**, 281–294, DOI: **10.1038/nchem.1889**.

10 E. Kovalenko, M. Vilaseca, M. Díaz-Lobo, A. N. Masliy, C. Vicent and V. P. Fedin, Supramolecular Adducts of Cucurbit[7]uril and Amino Acids in the Gas Phase, *J. Am. Soc. Mass Spectrom.*, 2016, **27**, 265–276, DOI: **10.1007/s13361-015-1274-z**.

11 G. Carroy, V. Lemaur, C. Henoumont, S. Laurent, J. De Winter, E. De Pauw, J. Cornil and P. Gerbaux, Flying Cages in Traveling Wave Ion Mobility: Influence of the Instrumental Parameters on the Topology of the Host–Guest Complexes, *J. Am. Soc. Mass Spectrom.*, 2018, **29**, 121–132, DOI: **10.1007/s13361-017-1816-7**.

12 S. C. Habibi and G. Nagy, Assessing the use of host-guest chemistry in conjunction with cyclic ion mobility separations for the linkage-specific characterization of human milk oligosaccharides, *Int. J. Mass Spectrom.*, 2023, **483**, 116977, DOI: **10.1016/j.ijms.2022.116977**.

13 J. Lee, S. Jang, M. Kim, D. R. Boraste, K. Kim, K. M. Park and J. Seo, Trapping Alkali Halide Cluster Ions Inside the Cucurbit[7]uril Cavity, *J. Phys. Chem. Lett.*, 2022, **13**, 9581–9588, DOI: **10.1021/acs.jpclett.2c02583**.

14 J. Lee, H. Kim, H. Lee, D. R. Boraste, K. Kim and J. Seo, Protomer of Imipramine Captured in Cucurbit[7]uril, *J. Phys. Chem. A*, 2023, **127**, 10758–10765, DOI: **10.1021/acs.jpca.3c04556**.

15 M. M. Zimnicka, Structural studies of supramolecular complexes and assemblies by ion mobility mass spectrometry, *Mass Spectrom. Rev.*, 2024, **43**, 526–559, DOI: **10.1002/mas.21851**.

16 J. Lee, Y. Ahn, M. Kim and J. Seo, Isomerism of Cyclodextrin Tetramer Induced by Alkali Halide Cluster Ions Observed by Ion Mobility Spectrometry–Mass Spectrometry, *J. Am. Soc. Mass Spectrom.*, 2024, **35**, 622–630, DOI: **10.1021/jasms.3c00441**.

17 D. V. Dearden, T. A. Ferrell, M. C. Asplund, L. W. Zilch, R. R. Julian and M. F. Jarrold, One Ring to Bind Them All: Shape-Selective Complexation of Phenylenediamine Isomers with Cucurbit[6]uril in the Gas Phase, *J. Phys. Chem. A*, 2009, **113**, 989–997, DOI: **10.1021/jp808771n**.

18 M. J. Frisch, G. W. Trucks, H. B. Schlegel, G. E. Scuseria, M. A. Robb, J. R. Cheeseman, G. Scalmani, V. Barone, G. A. Petersson, H. Nakatsuji, X. Li, M. Caricato, A. V. Marenich, J. Bloino, B. G. Janesko, R. Gomperts, B. Mennucci, H. P. Hratchian, J. V. Ortiz, A. F. Izmaylov, J. L. Sonnenberg, D. Williams-Young, F. Ding, F. Lipparini, F. Egidi, J. Goings, B. Peng, A. Petrone, T. Henderson, D. Ranasinghe, V. G. Zakrzewski, J. Gao, N. Rega, G. Zheng, W. Liang, M. Hada, M. Ehara, K. Toyota, R. Fukuda, J. Hasegawa, M. Ishida, T. Nakajima, Y. Honda, O. Kitao, H. Nakai, T. Vreven, K. Throssell, J. A. Montgomery Jr., J. E. Peralta, F. Ogliaro, M. J. Bearpark, J. J. Heyd, E. N. Brothers, K. N. Kudin, V. N. Staroverov, T. A. Keith, R. Kobayashi, J. Normand, K. Raghavachari, A. P. Rendell, J. C. Burant, S. S. Iyengar, J. Tomasi, M. Cossi, J. M. Millam, M. Klene, C. Adamo, R. Cammi, J. W. Ochterski, R. L. Martin, K. Morokuma, O. Farkas, J. B. Foresman and D. J. Fox, *Gaussian 16 Rev. C.01*, Wallingford, CT, 2016.

19 C. Adamo, M. Cossi and V. Barone, An accurate density functional method for the study of magnetic properties: the PBE0 model, *J. Mol. Struct. THEOCHEM*, 1999, **493**, 145–157, DOI: **10.1016/S0166-1280(99)00235-3**.

20 S. Grimme, A. Hansen, J. G. Brandenburg and C. Bannwarth, Dispersion-Corrected Mean-Field Electronic Structure Methods, *Chem. Rev.*, 2016, **116**, 5105–5154, DOI: **10.1021/acs.chemrev.5b00533**.

21 F.-M. Tao, The counterpoise method and bond functions in molecular dissociation energy calculations, *Chem. Phys. Lett.*, 1993, **206**, 560–564, DOI: **10.1016/0009-2614(93)80183-P**.

22 Y. Tantirungrotechai, K. Phanasant, S. Roddecha, P. Surawatanawong, V. Sutthikhum and J. Limtrakul, Scaling factors for vibrational frequencies and zero-point vibrational energies of some recently developed exchange-correlation functionals, *J. Mol. Struct. THEOCHEM*, 2006, **760**, 189–192, DOI: **10.1016/j.theochem.2005.12.007**.

23 B. H. Besler, K. M. Merz Jr. and P. A. Kollman, Atomic charges derived from semiempirical methods, *J. Comput. Chem.*, 1990, **11**, 431–439, DOI: **10.1002/jcc.540110404**.

24 I. Campuzano, M. F. Bush, C. V. Robinson, C. Beaumont, K. Richardson, H. Kim and H. I. Kim, Structural Characterization of Drug-like Compounds by Ion Mobility Mass Spectrometry: Comparison of Theoretical and Experimentally Derived Nitrogen Collision Cross Sections, *Anal. Chem.*, 2012, **84**, 1026–1033, DOI: **10.1021/ac202625t**.

25 H. Kim, H. I. Kim, P. V. Johnson, L. W. Beegle, J. L. Beauchamp, W. A. Goddard and I. Kanik, Experimental and Theoretical Investigation into the Correlation between Mass and Ion Mobility for Choline and Other Ammonium Cations in N2, *Anal. Chem.*, 2008, **80**, 1928–1936, DOI: **10.1021/ac701888e**.

26 V. Shrivastav, M. Nahin, C. J. Hogan and C. Larriba-Andaluz, Benchmark Comparison for a Multi-Processing Ion Mobility Calculator in the Free Molecular Regime, *J. Am. Soc. Mass Spectrom.*, 2017, **28**, 1540–1551, DOI: **10.1007/s13361-017-1661-8**.

27 N. I. Saleh, A. L. Koner and W. M. Nau, Activation and Stabilization of Drugs by Supramolecular pKa Shifts: Drug-Delivery Applications Tailored for Cucurbiturils, *Angew. Chem., Int. Ed.*, 2008, **47**, 5398–5401, DOI: **10.1002/anie.200801054**.

